Role of Membrane Curvature on the Activation/Deactivation of Carnitine Palmitoyltransferase 1A: A Coarse Grain Molecular Dynamic Study

Ezequiel N. Frigini, Exequiel E. Barrera, Sergio Pantano, Rodolfo D. Porasso

PII: S0005-2736(19)30240-8

DOI: https://doi.org/10.1016/j.bbamem.2019.183094

Reference: BBAMEM 183094

To appear in: *BBA - Biomembranes*

Received date: 7 May 2019

Revised date: 20 September 2019

Accepted date: 23 September 2019

Please cite this article as: E.N. Frigini, E.E. Barrera, S. Pantano, et al., Role of Membrane Curvature on the Activation/Deactivation of Carnitine Palmitoyltransferase 1A: A Coarse Grain Molecular Dynamic Study, *BBA - Biomembranes*(2019), https://doi.org/10.1016/j.bbamem.2019.183094

Role of Membrane Curvature on the Activation/Deactivation of Carnitine Palmitoyltransferase 1A: A Coarse Grain Molecular Dynamic Study

Ezequiel N. Frigini[a], Exequiel E. Barrera[b], Sergio Pantano[b], Rodolfo D. Porasso[a,*]

[a]*Instituto de Matemáticas Aplicada San Luis (IMASL), CONICET, Facultad de Ciencias Físico Matemáticas y Naturales, Universidad Nacional de San Luis, Av. Ejército de los Andes 950, 5700 San Luis, Argentina*
[b]*Biomolecular Simulations Group, Institut Pasteur de Montevideo, Mataojo 2020, 11400 Montevideo, Uruguay*

Abstract

Carnitine Palmitoyltransferase 1A (CPT 1A) is an enzyme anchored to the outer mitochondrial membrane (OMM), where it regulates the passage of fatty acids into the mitochondria and intervenes in the process of β-oxidation of long-chain fatty acids. Although CPT 1A is inhibited by malonyl-CoA, its activity is also modulated by the curvature of OMM. This modulation depends on the behavior of the N-terminal domain (NTD), which can be adsorbed onto the OMM (nonactive CPT 1A) or interacting with the C-terminal domain (active CPT 1A). Aimed to provide mechanistic insights on the regulatory mechanism of CPT 1A, we studied the influence of the bilayer curvature on the NTD behavior through a series of coarse-grained (CG) molecular dynamics simulations using curved and planar membranes.

*Corresponding author

Comparative analysis suggests that the main determinant for the activation/deactivation of the enzyme is the tilt angle orientation of the transmembrane (TM) domains. Planar membranes induce a wide variation on the tilt angle orientation of TM helices, while curved geometries promote small angles with the membrane normal. Our results identify the first TM domain as an important component of the membrane sensing mechanism.

Keywords: Carnitine palmitoyltransferase 1A, Lipid bilayer curvature, Molecular dynamics, Coarse grain model

1. Introduction

Biological membranes are flexible barriers that delimit the cell and its inner compartments. Membrane curvature is important in defining the morphology of the cells, which can experience significant variations upon migration, immune responses, infection, apoptosis, etc. Among others, the Bin/Anphiphylin/Rvs (BAR) protein domains are involved in many of these processes. Different experiments and multiscale molecular simulations identified the physical parameters that control the interplay between BARs and membranes.[1, 2, 3] Among these features, the shape of the membrane seems to be crucial. Clearly, BAR protein domains are not the only ones related to membrane curvatures. The activity of several enzymes (Protein kinase C (PKC), Phospholipase C-delta1 (PLCδ1), Tafazzin) is associated with the curvature properties of phospholid bilayers.[4] Another relevant enzyme is Carnitine palmitoyltransferase 1 (CPT 1), which is recognized for its important role in the maintenance of cellular functions in eukaryotes, as noted in previous studies.[5, 6, 7] Its main regulatory role is the inhibition by malonyl-

CoA, which is responsible for controlling the speed of intramitochondrial fatty acid β-oxidation. CPT 1 senses also the availability of fatty acids and glucose. This role is very important in various functions such as the response to ischemia in the cardiac muscle[8] and the control of insulin secretion in pancreatic β-cells.[9]

CPT 1 family includes other carnitine palmitoyl and acetyltransferases that have different isoforms: CPT 1A, CPT 1B, CPT 1C, CPT, CPTIC 1B.[10, 11] CPT 1A is located in the outer membrane of the mitochondria (OMM).[12, 13] Although its full structure is not known, its topological organization has been the focus of different experimental studies.[14, 15] In particular, Fraser et. al,[16] showed that it contains two transmembrane domains (TMD1 and TMD2) connected by a linker region exposed to the inter-membrane space, while both the N-terminal and C-terminal domains (NTD and CTD, respectively) are exposed on the cystolic side of the membrane (see Figure 1). Based on the functional properties of CPT 1, Rao et al,[17] showed that the NTD may populate three different conformational states: *i*) associated with the CTD; *ii*) interacting with the OMM; or *iii*) freely fluctuating in the cytosol. Interactions in the two first cases suggested an amphiphilic character of the NTD. This inspired a series of NMR studies of the NTD in phospholipid micelles. The results showed some differences in characteristic peaks of H^N-N interactions varying according to the phospholipids composing the micelles and the curvature they elicited.[10, 17, 18] Taking all together, the current paradigm proposes that the amphiphilic character of the NTD allows an environment-dependent switching of interactions between the CTD or the OMM. When the NTD interacts with the CTD the

enzyme is activated, and is sensitive to modulation by the inhibitor malonyl-CoA. On the contrary, when the NTD interacts with the OMM, CPT1A is deactivated, becoming insensitive to malonyl-CoA.

The present work aims to gain novel insights on the role of the cell membrane curvature in the activation/deactivation of the CPT 1A from a theoretical point of view. Since the NTD is linked to the TMD1 by an unstructured region, conformational transitions are expected to happen within the multi ns timescale.[19] Hence, a conformational sampling within a timescale of ≈ 1 μs would be expected to provide a reasonable description of the actual dynamics of the NTD. However, an atomistic representation of the system including the protein embedded in the membrane and aqueous environment comprises over a million atoms. This relatively large size, added to the need to perform replicated simulations in order to obtain a glimpse on the statistics of the protein's dynamics and the influence of different starting configurations implies a prohibitive computational cost. Therefore, we resorted to perform a series of coarse-grained (CG) simulations. For this task we used the CG force field named SIRAH (Southamerican Initiative for a Rapid and Accurate Hamiltonian) for proteins[20] and its recent parameterization for lipids.[21] This CG force field is well suited for this study as it allows for a long-range description of electrostatics as well as an unbiased treatment of protein's secondary structure. Furthermore, it is ported to GROMACS (GROningen MAchine for Chemical Simulations) and fully profits from GPU (Graphics Processing Unit) acceleration. This approach, combined with a recent implementation to produce curved membrane patches using two different phospholipid species[22] provided a robust framework to the study of the dynamics

of the CPT 1A. Analysis of lipid bilayer curvature, radial distribution functions, hydration/dehydration, tilt angle orientation of TMD and secondary structure of the NTD, helped to provide new mechanistic information and identify the TMD as a key component of the membrane sensing mechanism of CPT 1A.

2. Methods

2.1. Construction of CPT 1A by homology modeling

Since the full-length structure of the protein is not determined, the initial coordinates of CPT 1A were constructed by homology modeling using the software Modeller.[23] As mentioned in the Introduction, CPT 1A is composed by a regulatory NTD connected to a catalytic CTD by two TM helices (Figure 1). Currently, only the NTD has been resolved experimentally (PDB ID: 2LE3,[17]). Therefore, we first searched for suitable templates for the CTD (residues 167-766) on the Protein Data Bank (`https://www.rscb.org`). Only 8 PDB structures showed identity levels above 30%, and from those the structure 1NDB, corresponding to the Murine Carnitine Acetyltransferase solved by X-ray diffraction at a resolution of 1.8 Å, was selected as template. The quality of the models generated by Modeller was first assessed using the Discrete Optimized Protein Energy (DOPE) scoring method;[24] and then validated on the Protein Structure Validation Server (PSVS) (`http://psvs-1_5-dev.nesg.org/`).[25] A Ramachandran plot of the best model is shown in Supplementary Material (Figure SM 1(a) and (b)).

To obtain the initial coordinates of TMD1 and TMD2, J_pred[26] was first

used to predict the secondary structure elements. This prediction was used as the input for the PREDDIMER server[27] to generate a model of the TM1 and TM2 helices (spanning residues 58-73 and 103-121, respectively). Finally, the loop regions connecting all the structured domains (NTD, TM1, TM2 and CTD) were completed using Modeller to obtain an all-atoms model of the full-length protein (Figure SM 3 in the Supplementary Material). These coordinates were mapped to CG using SIRAH Tools.[28]

2.2. Curved and Planar Lipid Bilayer

The word curvature in relation to the membrane structure is generally used to describe the physical shape of the cell membrane, that is, the round shape of the surface of the sphere. The curvature depends inversely on the size of the sphere, the larger the sphere is, the smaller the physical curvature. In this sense, a planar lipid bilayer has zero curvature and a micelle has a positive curvature.

The use of periodic boundary conditions in phospholipid bilayers makes the simulation of stable curvatures in membranes a non trivial problem. Different proportions of lipidic species per leaflet may be used to balance the dimensions of the simulating box. In addition, lipids like Phosphatidyl-Choline (PC) have a cylindrical shape and favor the formation of planar monolayers, whereas other species as PhosphatidylEthanolamine (PE) having a smaller headgroups, present a roughly conical shape (as shown in Figure 2(a)), imposing a negative curvature on the lipid monolayer. Although different numbers and species of lipids can be present in each leaflet, this may create tensions or pressure differences that cannot be relaxed by barostats, giving rise to frustrated systems.[29] Taking into account these facts, we fol-

lowed the procedure originally proposed by Magarkar et al.[22] to produce curved membrane patches. To this aim, we set up lipid patches containing 225 PalmitoylOleoylPhosphatidylCholine (POPC) molecules in one leaflet and 246 PalmitoylOleoylPhosphatidylEthanolamine (POPE) molecules in the other.[22, 30, 31, 32, 33, 34] As usual, the normal to the lipid surface oriented to the z-axis. Then, the patch was copied, translated and rotated, obtaining a lipid bilayer as shown in Figure 2(b). Then $\approx$ 13700 molecules of WT4 (SIRAH's water model)[35] were added for full-hydration of the lipid bilayer. Then restraints in the xy plane were applied to the glycerol bead (named BGL in SIRAH) of POPE lipids, and were allowed to move freely in the z-axis. If the restraints are removed, the lipids can diffuse freely, once the lipids have been mixed and the steady state has been reached, a planar binary lipid bilayer is obtained. It is worth to notice that although POPC and POPE account for 54% and 29% of the OMM lipid content, respectively,[36, 37] the use of only these two lipids clearly constitutes an oversimplification associated to the finite size of the simulation box.

2.3. System CPT 1A/Lipid Bilayer

Once the models of curved and planar lipid bilayer were constructed, the protein obtained in Section 2.1 was embedded into planar and curved membrane models. The Visual Molecular Dynamics program (VMD)[38] was used to insert both TMDs in the geometric center of the lipid bilayer and, subsequently, lipid molecules in close contact with the protein ($\leq$ 0.35 nm) were removed. Next, the system was hydrated ($\approx$ 26130 WT4 molecules) and 28 WT4 molecules were randomly replaced by Na^+ ions (in coarse-grained model) in order to balance the net charge of the simulation box. Afterwards,

the systems underwent energy minimization and two steps of equilibration as described below. For the first equilibration step, whole beads of the protein were restrained in xyz coordinates and the lipid phosphate groups (named BFO in SIRAH) were restrained only in the z-coordinate. In the second step of the equilibration, only the beads of the backbone of the protein were restrained in xyz coordinates, allowing the free movement of the rest of the protein. Each simulation was carried out for 5 ns at a temperature of 313 K. After the second equilibration simulation, the coordinates of the system were used as a starting point for productive simulations with and without restraints on the BGL beads of the lipids molecules in absence of restraints on the protein. The simulation time for each system was 1 μs at a temperature of 313 K. The convergence of areas per lipid (APL)[39] and Root Mean Square Deviations (RMSD) of the protein were used as indicators of the stability of the system (Figure 3).

2.4. Computational details

All MD simulations were performed at the CG level using the SIRAH force field[40] version 2.0, running on the GROMACS 4.6.7 software package.[41, 42, 43] Once the lipid bilayers were constructed (see Section 2.2), a steepest descent algorithm energy minimization was carried out followed by MD equilibration in the NVT ensemble. Finally, productive MD simulations were carried out for 1 μs at a reference temperature of 313 K, well above the transition temperature of POPC (270 K) and POPE ($\approx$ 280 K).[44] The v-rescale thermostat[45] with a coupling constant of 1.0 ps was used. A semi-isotropic pressure coupling in x and y (the z axis of the simulation box corresponds to the bilayer normal) with a Berendsen barostat[46] with a coupling con-

stant of 1.0 ps, a compressibility value of 4.5×10^{-5} bar^{-1}, and a reference pressure of 1 bar was used. Electrostatics/Coulombic interactions were calculated using particle mesh Ewald[47] with a cut off length of 1.2 nm; van der Waal's interactions cut off was set at 1.2 nm. Aimed to enhance the conformational sampling, six independent replicas were simulated in planar and curved bilayers considering different orientations and initial coordinates of the enzyme in the membrane as well as different initial coordinates of the lipid bilayer and seed values for the initials velocities. The programs `g_lomepro`[48], MD Analysis[49, 50, 51] and pybilt (`https://github.com/blakeaw/PyBILT`) were used for the analysis of the different properties. The final results of each property analyzed, correspond to the average over the different MD simulations, and the corresponding statistical error were calculated as the standard deviation.

3. Results and Discussions

3.1. Membrane Curvature Calculations

In order to calculate the lipid bilayer curvature, we used the program `g_lomepro`, which calculates the mean curvature J as:[48, 52]

$$J = \frac{EN + GL - 2FM}{2(EG - F)^2} \tag{1}$$

where: $E = S_x \cdot S_x$, $F = S_x \cdot S_y$ and $G = S_y \cdot S_y$, defining the first order derivative as: $S_x = \partial S/\partial x$ and $S_y = \partial S/\partial y$ for every grid cell (x, y) for both leaflets. The unit normal to the surface at every grid point is calculated as $\mathbf{N} = (S_x \times S_y)/||S_x \times S_y||$. Then, the second order derivatives are calculated as, $S_{xx} = \partial^2 S/\partial x^2$, $S_{yy} = \partial^2 S/\partial y^2$ and $S_{xy} = \partial^2 S/\partial x \partial y$. This enables the estimation of: $L = S_{xx} \cdot \mathbf{N}$, $M = S_{xy} \cdot \mathbf{N}$ and $N = S_{yy} \cdot \mathbf{N}$.

Figure 4(a) shows the results of the curvature calculation using equation (1) for both membrane models with and without the CPT 1A, at one moment of the simulation time (arbitrarily chosen). The lipid bilayer without restraint in the BGL of the POPE lipids is almost planar except for some small temporal fluctuations. Which can be reduced if the average curvature is calculated over the simulation time. The same behavior is observed in the presence of the CPT 1A, except for the permanent positive curvature on both sides of the bilayer in the region where the protein is anchored (see also panels 4(b) and 4(d) for molecular visualizations). In contrast, when restraints are applied, well-defined curved membrane patches are clearly recognizable both in presence and absence of the protein (Figure 4 (c) and (e), respectively).

3.2. N-Terminal-Lipid Interactions

The radial distribution function (RDF) is often used to identify interactions between neighboring atoms. In this regard, the RDF is defined as:

$$g(r) = \frac{N(r)}{4\pi r^2 \rho \delta r} \tag{2}$$

where, $N(r)$ is the number of atoms in a spherical shell at distance r and thickness δr from a reference atom, and ρ is the number density taken as the ratio of atoms to the volume of the computing box.

To further quantify a possible interaction between the N-terminal and the lipid heads, the RDF of the phosphate beads of both types of lipids, POPE and POPC, were calculated around the residues 10 to 40 of the N-terminal of CPT 1A enzyme for the last 200 ns of the simulation time. These calculations are depicted in Figure 5(a). The integral over the distance to

the first minimum of the RDF determines how many lipids are nearby. The results of these calculations show that the number of lipids around the NTD is higher when the lipid bilayer is planar than curved. This reveals that the planar lipid bilayer exhibits more interactions than the curved one. These conclusions can also be observed in Figure 4(d) and (e), which visualize that the N-terminal interacts with the planar lipid bilayer (Figure 4(d)), while it prefers the interaction with the C-terminal if the membrane patch is curved (Figure 4(e)). These findings agree with the experimental results previously shown by Rao et. al.[17]

A concomitant piece of information is obtained from the analysis of the RDF of WT4 molecules (water model in SIRAH) around the same residues of the N-terminal. Figure 5(b) shows the results of the $g(r)$ corresponding to the first 150 ns (open symbols) and the last 200 ns (solid symbols). From these results, it can be observed that at the beginning of the simulations the residues of the N-terminal are hydrated to a similar extent, independently of the curvature of the lipid bilayer. However, in the last 200 ns of the total simulation time, the residues of the NTD underwent curvature dependent dehydration. If the lipid bilayer is curved, the dehydration process is less marked because the NTD interacts with the CTD (as can be seen in Figure 4(e)). This interaction between NTD and CTD also causes the loss of sensitivity of the C-terminal domain to malonyl-CoA.[53, 18, 10] Moreover, if the lipid bilayer is planar, the N-terminal exhibits a greater dehydration, which is a consequence of the interaction with the lipids (shown in Figures 4(d) and 5(a)).

In order to gain a deeper insight on the number of solvent interacting

with the N-terminal residues, we calculated the number of hydrating water molecules by numerically integrating the corresponding RDF up to the first minimum (r_{fm}) according to:

$$N_i = 4\pi\rho \int_0^{r_{fm}} g_i(r) r^2 dr \tag{3}$$

The hydration numbers (N_i) for the N-terminal residues of CPT 1A are depicted in Figure 6(a) and (b) for the curved and planar lipid bilayers, respectively. In the first case, it can be observed that the terminal residues undergo very little dehydration, while for the planar lipid bilayer (Figure 6(b)), the dehydration suffered by many residues is remarkable. In a deeper analysis, it can be seen that not all residues are dehydrated. In particular, some residues that belong to the $\alpha 2$ structure (see Section 3.4) remain hydrated, owing to the amphipahtic character of this segment.

3.3. Transmembrane Domain Behavior

The tilt angle orientation of the transmembrane domain, defined as the angle between the major axis of the helix and the bilayer normal ($\hat{z}$), provides important information to rationalize the protein-membrane interplay. Therefore, we computed the time evolution of the tilt angle of TMD1 and the membrane normal using MD Analysis.[49, 50, 51] The results of the time evolution of the tilt angle orientation, for each of the MD replicas, are represented in the left column of Figure 7. As it can be observed, the TMD1 of the replicas of simulations in planar membranes, tend to sample higher and more spread values centered around 40°. This is particularly evident considering the probability distributions calculated over the second half of the simulations (see Figure 7 right panel). However, when simulations are performed

on curved bilayers, they show a tendency to sample lower values, with a major peak above 10°. As evidenced by a different orange tonality in Figure 7, this is the case for all but two replicas. In those two particular replicas, despite being inserted in curved membranes, the initial conformation placed the TMD1 oriented along the saddle point of the curved membrane, where there is no curvature (see Supplementary Material Figure SM 5). Hence, locally, the TMD1 of CPT 1A is sensing a planar membrane, maintaining a high tilt angle value. It is important to underline that this effect is an unforeseen but interesting result of the method used to produce curved membranes, as it provides a control for our hypothesis.[54, 55, 56] In our interpretation, the TMDs act as the curvature sensor. That is, if the lipid bilayer is curved, the tilt angle orientation of the TMD1 remains constant (in our case $\approx 10°$) and the NTD interacts with the CTD, which implies that the enzyme is active. If the lipid bilayer is planar, then the tilt angle orientation of the TMD1 can raise significantly. Therefore, the N-terminal can move towards the membrane and get adsorbed, inducing the enzyme deactivation (see Figure 8). Under this perspective, and considering the curvature gradients shown in Figure 4, this could lead to the speculation that the sensing capacity of the protein is quite local and restricted to a distance involving a few phospholipids. Further analysis of the relative orientation of the enzyme in relation to the membrane curvatures revealed no clear preferences in the different replicas.

In order to obtain an insight about the behavior of the TMDs, the radial distribution functions (equation (2)) were calculated around both TMDs of CPT 1A of the two types of lipids, for the first 150 ns and for the last 200

ns of the simulation time, both for the planar and curved lipid bilayer. In the case of the curved lipid bilayer (Figure 9 (a)), it is observed that the $g(r)$ remains similar for the two types of lipids. In addition, although some preference of the TMDs for the POPE lipid is barely noticed, they remain without major changes, for the initial and for the latest part of the simulation. In the presence of the planar lipid bilayer, a different behavior of $g(r)$ can be observed. First, a clear preference of the transmembrane domains can be observed for the POPE lipid over the POPCs. Moreover, an increase in the coordination with the lipids can be observed once the N-terminal interacts with the lipid bilayer. This preference for POPE lipids is due to steric instead of electrostatic interactions, since the head group of the lipid has a conical shape that facilitates the interaction with the enzyme.

3.4. Secondary Structure of Nα and Nβ Behavior

Rao et al.[17] have shown that there is a correlation between the secondary structure and the N-terminal functionality. Using multidimensional heteronuclear NMR spectroscopy, they elucidated that the structure Nβ (extended or β-sheet) is adopted if the membrane is curved, while the Nα (α-helix) exists when the NTD is adsorbed on the planar OMM. In the present work, we have determined the secondary structure of the N-terminal along the simulation time, in the presence of both lipid bilayer (planar and curved).

To gain a deeper insights on the conformational behavior of the NTD at nearly atomistic detail, we backmapped the CG trajectory using the backmapping utilities of SIRAH Tools[28]. In Figure 10(a), we show the schematic representation of the NTD structure. Three secondary structure elements can be found in the NTD: β1 (The10-Thr15), β2 (Gly18-Leu23),

α2 (His25-Ser38) and the structure α1 which is adopted under certain circumstances and is comprised between residues Ala4-Ala7. Figure 10(b) and (c) plot the time evolution of the secondary structures α1, α2, β1 and β2 of the NTD in the presence of a curved and planar lipid bilayer, respectively. In these Figures, cyan represents coil, purple α-helix, and yellow extended conformations.

It is known that the secondary structure of the α-helix is conserved if it is adsorbed on a certain surface, whereas if the α-helix is free in the bulk solution this secondary structure is not stable, and conformational transition to coil can occur. From the analysis of the secondary structure of α1 (residues 1-10 of Figure 10(b) and (c)), it is observed that the helical state depends on weather the NTD interacts with the CTD or with the lipid bilayer. Although the NTD interacts with the CTD when the enzyme is activated, residues 1-10 do not and remain free in the cytosol, remaining mainly in coil (Figure 10(b)). On the other hand, when the NTD interacts with a planar lipid bilayer by deactivating the carnitine activity, the Ala4-Ala7 residues adsorb on the surface of the bilayer, which favors the formation of the secondary structure, as shown in the Figure 10(c). In contrast, the α2 structure is conserved independently of the curvature of the membrane. Therefore, for any of the possible states of carnitine, the residues 25-39 of the NTD are adsorbed either on the CTD or the planar lipid bilayer, preserving its secondary structure along the simulation time. Finally the structures β1 and β2 also conserved independently of the lipid bilayer curvature.

4. Conclusions

We used CG simulations to investigate the role of the lipid bilayer curvature in the activation/deactivation of the CPT 1A. The simulations provided a valuable insight into the interaction between the CPT 1A and the lipid bilayer. The analysis of the tilt angle of the TMD suggests that TMD behave as the sensors of the curvature of the lipid bilayer. In this sense, the behavior of the tilt angle of TMD seems to act as the structural switch for the activation/deactivation of carnitine. This happens in combination with the amphiphilic structure of the NTD. When the lipid bilayer is curved, the tilt angle of the transmembrane domains remains stable, blocking the interaction of the NTD with the membrane. The solvated NTD is thus free to bind on the CTD, leading the enzyme to the active state. If the lipid bilayer is planar the tilt angle orientations can change over a wide range, favoring conformations in which the NTD is prone to interact with the lipid bilayer (Figure 8). This requires the partial desolvation of the NTD to establish favorable amphipathic interactions with the aqueous and membrane phases simultaneously. Once the NTD is adsorbed onto the membrane the enzyme turns into the deactivated state.

Acknowledgement

E.N.F. is beneficiary of a doctoral fellowship of CONICET, E.E.B. is beneficiary of a postdoctoral fellowship of CONICET, S.P. is a researcher of the National Scientific Program of ANII (SNI) and R.D.P. is a staff member of CONICET.

The authors wish to acknowledge the Computer Center staff of the *Instituto de Matemática Aplicada San Luis* for their technical support in carrying out the simulations of this work. Some of the simulations were performed on the National Uruguayan Centre for Supercomputing, ClusterUY. We gratefully acknowledge the support of NVIDIA Corporation with the donation of the Titan Xp GPU used for this research.

Disclosure statement

The authors declare that they have no conflict of interest.

Funding

This work was partially funded by PROICO 03-1116 from Universidad Nacional de San Luis, Argentina and by FOCEM (MERCOSUR Structural Convergence Found), COF 03/11.

References

[1] C. Mim, V. M. Unger, Membrane curvature and its generation by bar proteins, Trends in Biochemical Sciences 37 (12) (2012) 526 – 533. doi:10.1016/j.tibs.2012.09.001.

[2] M. Simunovic, G. A. Voth, A. Callan-Jones, P. Bassereau, When physics takes over: Bar proteins and membrane curvature, Trends in Cell Biology 25 (12) (2015) 780 – 792. doi:10.1016/j.tcb.2015.09.005.

[3] Z. Jarin, F.-C. Tsai, A. Davtyan, A. J. Pak, P. Bassereau, G. A. Voth, Unusual organization of i-bar proteins on tubular and vesicular membranes, Biophys J 117 (2019) 1–10. doi:10.1016/j.bpj.2019.06.025.

[4] R. M. Epand, K. D'Souza, B. Berno, M. Schlame, Membrane curvature modulation of protein activity determined by nmr, BBA-Biomembranes 1848 (1, Part B) (2015) 220–228. doi:10.1016/j.bbamem.2014.05.004.

[5] J. D. McGarry, Disordered metabolism in diabetes: Have we underemphasized the fat component?, Cell Biochem 55 (1994) 29–38.

[6] G. M. Reaven, The fourth musketeer - from alexandre dumas to claude bernard, Diabetologia 38 (1995) 3–13.

[7] V. A. Zammit, Role of insuline in hepatic fatty acid partitionig: emerging concepts, Biochem J 314 (1996) 1–14.

[8] G. D. Lopaschuk, D. D. Belke, J. Gamble, I. Toshiyuki, B. O. Schönekess, Regulation of fatty acid oxidation in the mammalian heart in health and disease, Biochim Biophys Acta 1213 (1994) 273–276.

[9] M. Prentki, B. E. Corkey, Are the β-cell signaling molecules malonyl-coa and cytosolic long-chain acyl-coa implicated in multiple tissue defects of obesity and niddm?, Diabetes 45 (1996) 273–283.

[10] N. Casals, V. A. Zammit, L. Herrero, R. Fadó, R. Rodríguez-Rodríguez, D. Serra, Carnitine palmitoyltransferase 1c: From cognition to cancer, Prog Lipid Res 134 (2016) 134–148.

[11] J. D. McGarry, N. F. Brown, The mitochondrial carnitine palmitoyltransferasa system. from concept to molecular analysis, Eur J Biochem 244 (1997) 1–14.

[12] M. S. Murthy, S. V. Pande, Malonyl-coa binding site and the overt carnitine palmitoyltransferase activity reside on the opposite sides of the outer mitochondrial membrane, P Natl Acad Sci 84 (1987) 378–382.

[13] M. P. Kolodziej, V. A. Zammit, Re-evaluation of the interaction of malonyl-coa with the rat liver mitochondrial carnitine palmitoyltransferase system by using purified outer membranes, Biochem J 267 (1990) 85–90.

[14] M. P. Kolodziej, V. A. Zammit, Mature carnitine palmitoyltransferase i retains the n-terminus of the nascent protein in rat liver, FEBS Letters 327 (1993) 294–296.

[15] N. A. E. Steenaart, J. R. Silvius, G. C. Shore, An amphiphilic lipid-binding domain influences the topology of a signal-anchor sequence in the mitochondrial outer membrane, Biochemistry 35 (1996) 3796–3771.

[16] F. Fraser, C. G. Corstorphine, V. A. Zammit, Topology of carnitine palmitoyltransferase i in the mitochondrial outer membrane, Biochem J 323 (1997) 711–718.

[17] J. N. Rao, G. Z. L. Warren, S. Estolt-Povedano, V. A. Zammit, T. S. Ulmer, An environment-dependent structural switch underlies the regulation of carnitine palmitoyltransferase 1a, J Biol Chem 286 (2011) 42545–42554.

[18] V. A. Zammit, Carnitine palmitoyltransferase 1: Central to cell function, IUBMB Life 60 (2008) 347–354.

[19] D. Haenni, F. Zosel, L. Reymond, D. Nettels, B. Schuler, Intramolecular distances and dynamics from the combined photon statistics of single-molecule fret and photoinduced electron transfer, J Phys Chem B 117 (2013) 13015 – 13028.

[20] M. R. Machado, E. E. Barrera, F. Klein, M. Sóñora, S. Silva, S. Pantano, The sirah 2.0 force field: Altius, fortius, citius, J Chem Theory Comput 15 (4) (2019) 2719–2733, pMID: 30810317. doi:10.1021/acs.jctc.9b00006.

[21] E. E. Barrera, M. R. Machado, S. Pantano, Fat sirah: Coarse-grained phospholipids to explore membrane-protein dynamics, J Chem Theory Comput (2019) In Press.doi:10.1021/acs.jctc.9b00435.

[22] A. Magarkar, P. Jurkiewicz, C. Allolio, M. Hof, P. Jungwirth, Increased binding of calcium ions at positively curved phospholipid membranes, J Phys Chem Lett 8 (2) (2017) 518–523. doi:10.1021/acs.jpclett.6b02818.

[23] B. Webb, A. Sali, Comparative protein structure modeling using modeller, Current Protocols in Bioinformatics 54 (2016) 5.6.1–5.6.37.

[24] M.-y. Shen, A. Sali, Statistical potential for assessment and prediction of protein structures, Protein Sci 15 (11) (2006) 2507–2524.

[25] A. Bhattacharya, R. Tejero, G. T. Montelione, Evaluating protein structures determined by structural genomics consortia, Proteins: Structure, Function, and Bioinformatics 66 (4) (2007) 778–795.

[26] A. Drozdetskiy, C. Cole, J. Procter, G. J. Barton, Jpred4: a protein secondary structure prediction server, Nucleic Acids Res 43 (W1) (2015) W389–W394.

[27] A. A. Polyansky, A. O. Chugunov, P. E. Volynsky, N. A. Krylov, D. E. Nolde, R. G. Efremov, Preddimer: a web server for prediction of transmembrane helical dimers, Bioinformatics 30 (2014) 889–890.

[28] M. R. Machado, S. Pantano, SIRAH tools: mapping, backmapping and visualization of coarse-grained models, Bioinformatics 32 (10) (2016) 1568–1570. doi:10.1093/bioinformatics/btw020.

[29] F. E. Herrera, S. Pantano, Structure and dynamics of nano-sized raft-like domains on the plasma membrane, J Chem Phys 136 (2012) 015103. doi:10.1063/1.3672704.

[30] V. Kumar, Complementary molecular shapes and additivity of the packing parameter of lipids, P Natl Acad Sci 88 (2) (1991) 444–448.

[31] S. Vanni, H. Hirose, H. Barelli, B. Antonny, R. Gautier, A sub-nanometre view of how membrane curvature and composition modulate lipid packing and protein recruitment, Nat Commun 5 (2014) 4916.

[32] A. Melcrová, S. Pokorna, S. Pullanchery, M. Kohagen, P. Jurkiewicz, M. Hof, P. Jungwirth, P. S. Cremer, L. Cwiklik, The complex nature of calcium cation interactions with phospholipid bilayers, Sci Rep-UK 6 (2016) 38035.

[33] P. L. Yang, Chapter 14 - metabolomics and lipidomics: Yet more ways your health is influenced by fat, in: M. G. Katze, M. J. Korth, G. L.

Law, N. Nathanson (Eds.), Viral Pathogenesis (Third Edition), third edition Edition, Academic Press, Boston, 2016, pp. 181 – 198. doi:10.1016/B978-0-12-800964-2.00014-8.

[34] K. J. Boyd, E. R. May, Bumpy: A model-independent tool for constructing lipid bilayers of varying curvature and composition, J Chem Theory Comput 14 (12) (2018) 6642–6652. doi:10.1021/acs.jctc.8b00765.

[35] L. Darré, M. R. Machado, P. D. Dans, F. E. Herrera, S. Pantano, Another coarse grain model for aqueous solvation: Wat four?, J Chem Theory Comput 6 (2010) 3793–3797.

[36] G. Daum, J. E. Vance, Import of lipids into mitochondria, Prog Lipid Res 36 (2-3) (1997) 103–130.

[37] E. M. Mejia, G. M. Hatch, Mitochondrial phospholipids: role in mitochondrial function, J Bioenerg Biomembr 48 (2) (2016) 99–112.

[38] W. Humphrey, A. Dalke, K. Schulten, VMD – Visual Molecular Dynamics, J Mol Graphics 14 (1996) 33–38.

[39] R. D. Porasso, J. J. López Cascales, A criterion to identify the equilibration time in lipid bilayer simulations, Papers in Physics 4 (2012) 040005.

[40] L. Darré, M. R. Machado, A. F. Brandner, H. C. González, S. Ferreira, S. Pantano, Sirah: A structurally unbiased coarse-grained force field for proteins with aqueous solvation and long-range electrostatics, J Chem Theory Comput 11 (2015) 723–739.

[41] H. J. C. Berendsen, D. van der Spoel, R. van Drunen, Gromacs: A message-passing parallel molecular dynamics implementation, Comp Phys Comm 91 (1995) 43–56.

[42] D. van der Spoel, E. Lindahl, B. Hess, G. Groenhof, A. E. Mark, H. J. C. Berendsen, Gromacs: fast, flexible, and free, J Comput Chem 26 (2005) 1701–1718.

[43] M. J. Abraham, T. Murtola, R. Schulz, S. Páll, J. C. Smith, B. Hess, E. Lindahl, Gromacs: High performance molecular simulations through multi-level parallelism from laptops to supercomputers, SoftwareX 1-2 (2015) 19–25.

[44] S. Leekumjorn, A. K. Sum, Molecular characterization of gel and liquid-crystalline structures of fully hydrated popc and pope bilayers, J Phys Chem B 11 (2007) 6026–6033.

[45] G. Bussi, D. Donadio, M. Parrinello, Canonical sampling through velocity rescaling, J Chem Phys 126 (2007) 014101.

[46] H. J. C. Berendsen, J. P. M. Postma, W. F. van Gunsteren, A. DiNola, J. R. Haak, Molecular dynamics with coupling to an external bath, J Chem Phys 81 (8) (1984) 3684 – 3690.

[47] T. A. Darden, D. York, L. Pedersen, Particle mesh ewald: an n-log(n) method for ewald sum in large systems, J Chem Phys 98 (1993) 10089–10092.

[48] B. R. Gapsys V, de Groot BL, Computational analysis of local membrane properties., J Comput Aided Mol Des 27 (2013) 845–858.

[49] M. Bansal, S. Kumar, R. Velavan, Helanal - a program to characterise helix geometry in proteins, J Biomol Struct Dyn 17 (2000) 811–819.

[50] S. Kumar, M. Bansal, Structural and sequence characteristics of long alpha-helices in globular proteins, Biophys J 71 (1996) 1574–1586.

[51] S. Kumar, M. Bansal, Geometrical and sequence characteristics of alpha helices in globular proteins, Biophys J 75 (1998) 1935–1944.

[52] J. M. Lee, Riemannian manifolds: an introduction to curvature, New York: Springer, 1997.

[53] J. D. McGarry, G. P. Mannaerts, D. W. Foster, A possible role for malonyl-coa in the regulation of hepatic fatty acid oxidation and ketogenesis, J Clin Invest 60 (1977) 265–270.

[54] G. Drin, J.-F. Casella, R. Gautier, T. Boehmer, T. U. Schwartz, B. Antonny, A general amphipathic α-helical motif for sensing membrane curvature, Nat Struct Molr Biol 14 (2007) 138–146.

[55] G. Drin, V. Morello, J.-F. Casella, P. Gounon, B. Antonny, Asymmetric tethering of flat and curved lipid membranes by a golgin, Science 320 (5876) (2008) 670–673.

[56] H. T. McMahon, E. Boucrot, Membrane curvature at a glance, J Cell Sci 128 (6) (2015) 1065–1070.

Figures

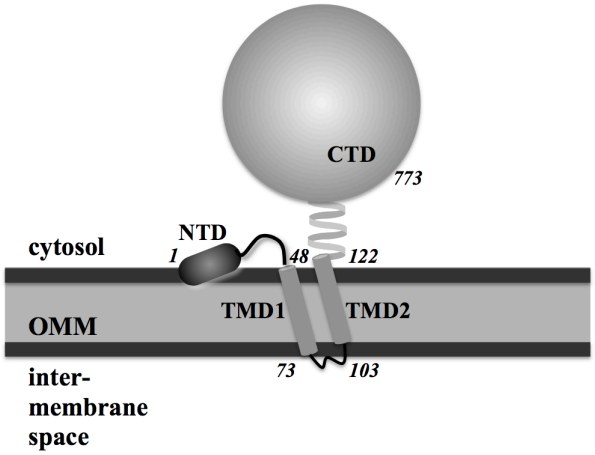

Figure 1: Schematic representation of the topology adapted from Fraser et al.[16]. The initial and/or final amino acids are indicated for: NTD, TMD1, TMD2 and CTD. Possible associated states of NTD are: OMM-associated (represented in this figure, corresponding to deactivation of the enzyme), CTD-associated (which corresponds to activation of the enzyme) or freely fluctuating in the cytosol.

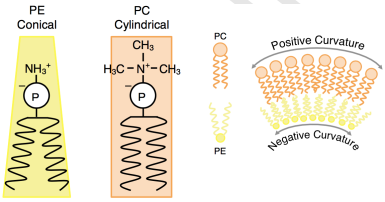

(a) Head group size.

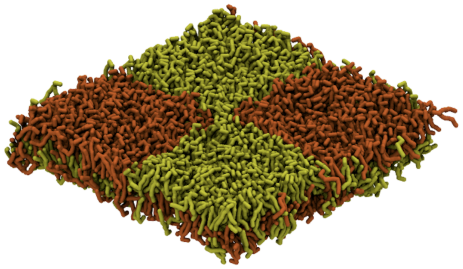

(b) Lipid bilayer composed by POPC (orange) and POPE (yellow).

Figure 2: (a) Different shape of the PC and PE lipids which induce a curvature on a binary lipid bilayer, positive curvature in the PC leaflet and negative in the PE leaflet. (b) The lipid bilayer formed by the four patches before applying the minimization protocol.

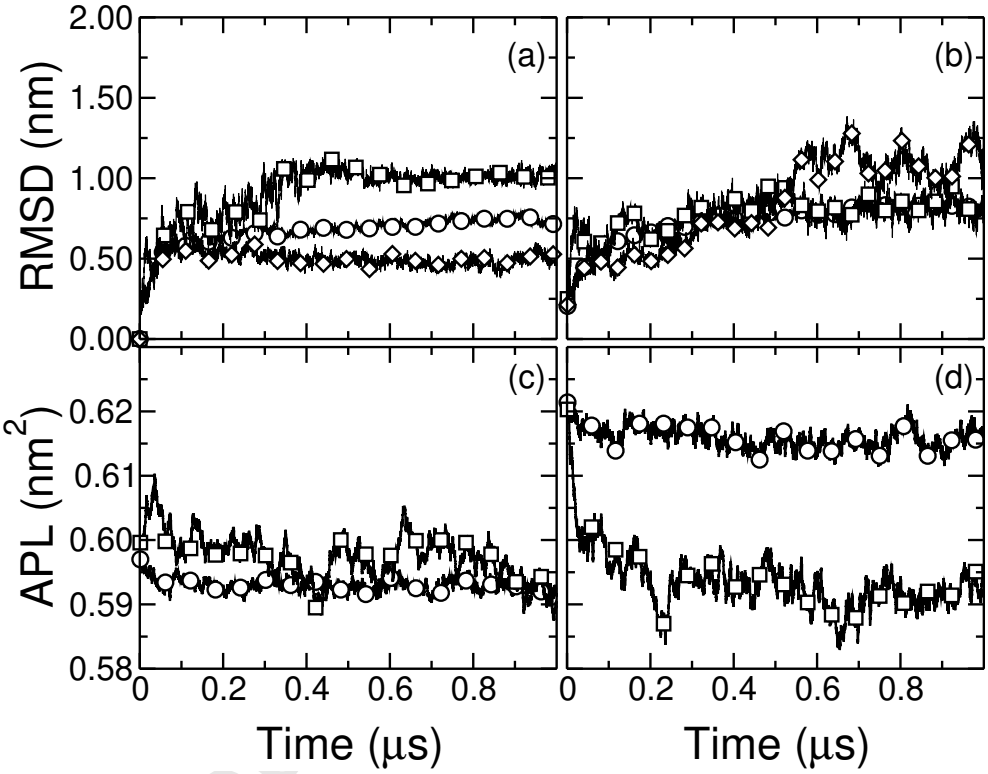

Figure 3: **Top row.** Root mean square deviation of atom distance □ NTD, ◯ CTD and ◊ TMDs. (a) Corresponds to the curved lipid bilayer and (b) to the planar lipid bilayer. **Bottom row.** Time evolution of the area per lipid for the lipid bilayer □ planar and ◯ curved. For the lipid bilayer: (c) in the presence of the CPT 1A and (d) in the absence of the CPT 1A .

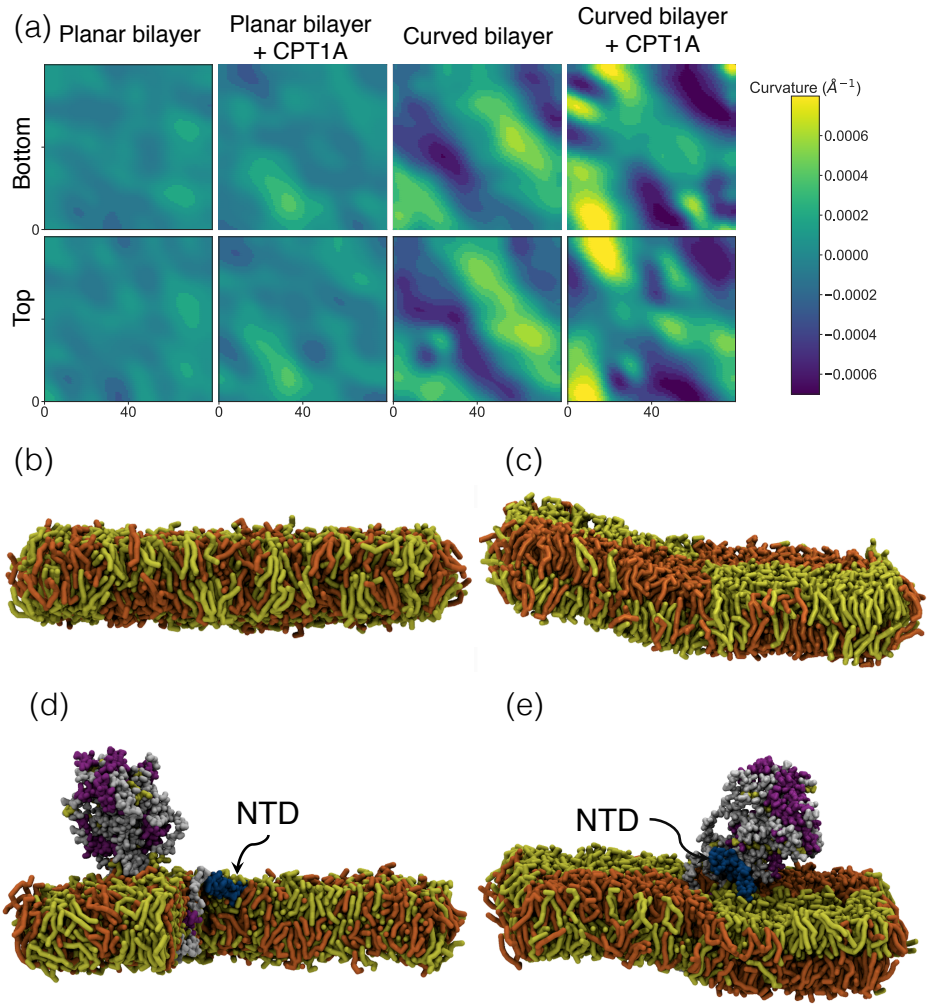

Figure 4: (a) Calculation of J for the lipid bilayer according equation (1) at a representative time of the MD simulation. Side-view snapshot of: (b) pure lipid bilayer without restraint in lipids, (c) pure lipid bilayer with restraint on POPE lipids, (d) lipid bilayer/CPT 1A without restraints in lipids and (e) lipid bilayer/CPT 1A with restraint on POPE lipids. For the CPT 1A, the NTD is colored in blue to highlight its location, on (d) some lipid were removed to unveil the location of the NTD adsorbed onto the lipid bilayer surface. Water molecules are omitted for clarity.

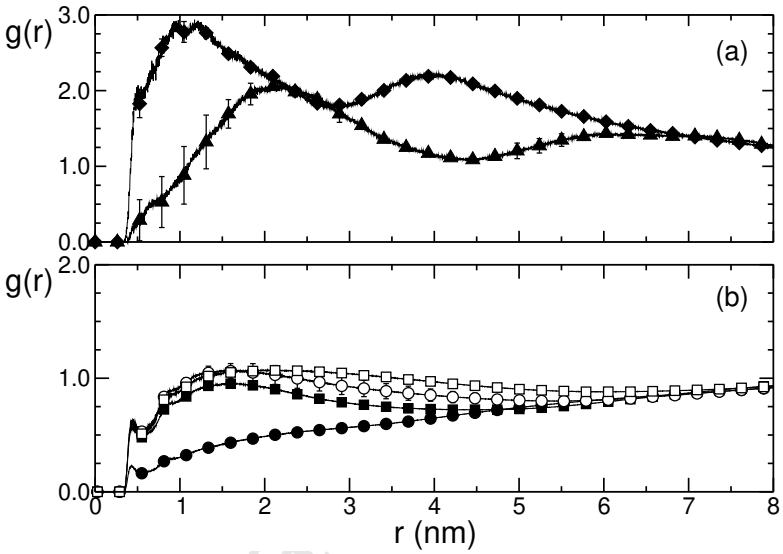

Figure 5: (a) Radial distribution function of phosphate beads of POPE and POPC around the residues 10 to 40 of the N-terminal of the CPT 1A enzyme. These RDF were computed for the last 200 ns of the simulations. Symbols: ▲ curved lipid bilayer and ♦ planar lipid bilayer. (b) Radial distribution function of WT4 (water model) around the residues 10 to 40 of the N-terminal of the CPT 1A enzyme. Symbols: for the first 150 ns, □ stands for curved lipid bilayer and ○ for planar lipid bilayer; for the last 200 ns, ■ stands for curved lipid bilayer and ● for planar lipid bilayer. The error bars are calculated as the standard deviation, which in some cases are the same size or smaller than the symbols.

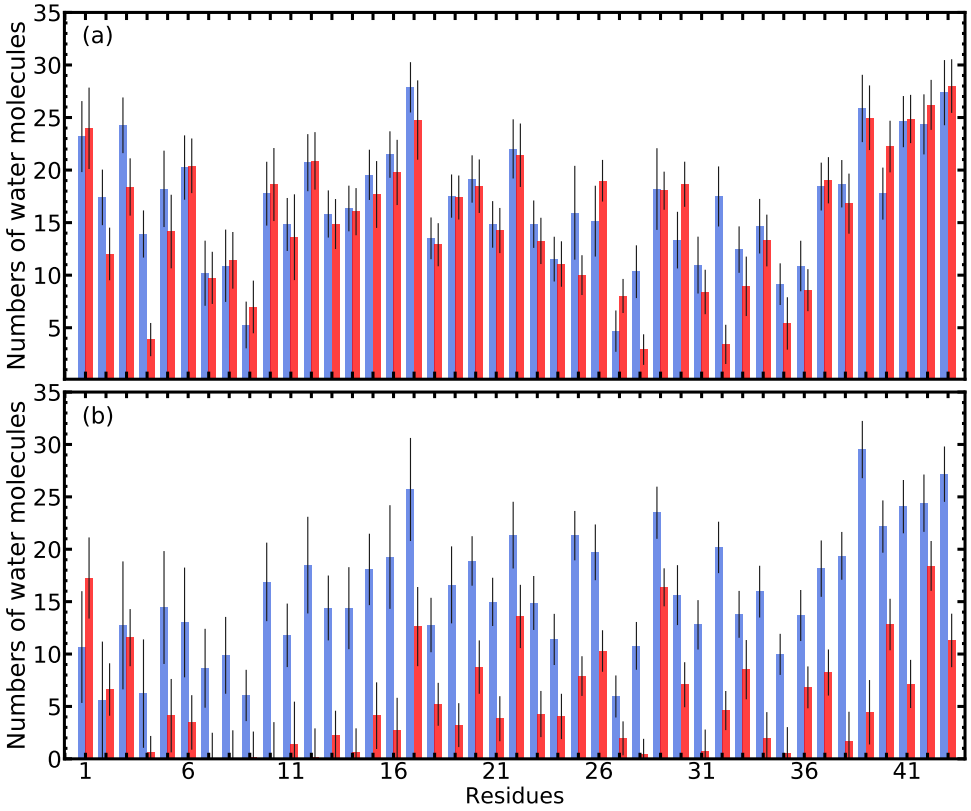

Figure 6: Hydration number for the residues belonging to the N-terminal of CPT 1A enzyme, corresponding to: (a) the curved lipid bilayer and (b) planar lipid bilayer. Color: Blue for the first 150 ns and red for the last 200 ns. Error bars represent the standard deviations.

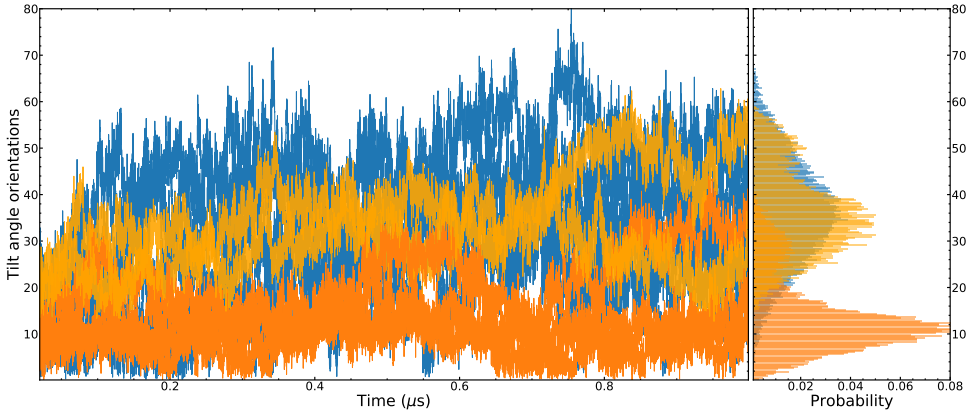

Figure 7: Left column. Tilt angle orientation of TMD1 of the CPT 1A in presence of a planar lipid bilayer (blue lines) and a curved lipid bilayer (in this case two different orange tonalities lines are used to distinguish the different behavior observed in the replicas). Right column. Probability distribution of the tilt angle orientation values calculated over the last 500 ns, considering all the repetitions of the simulations.

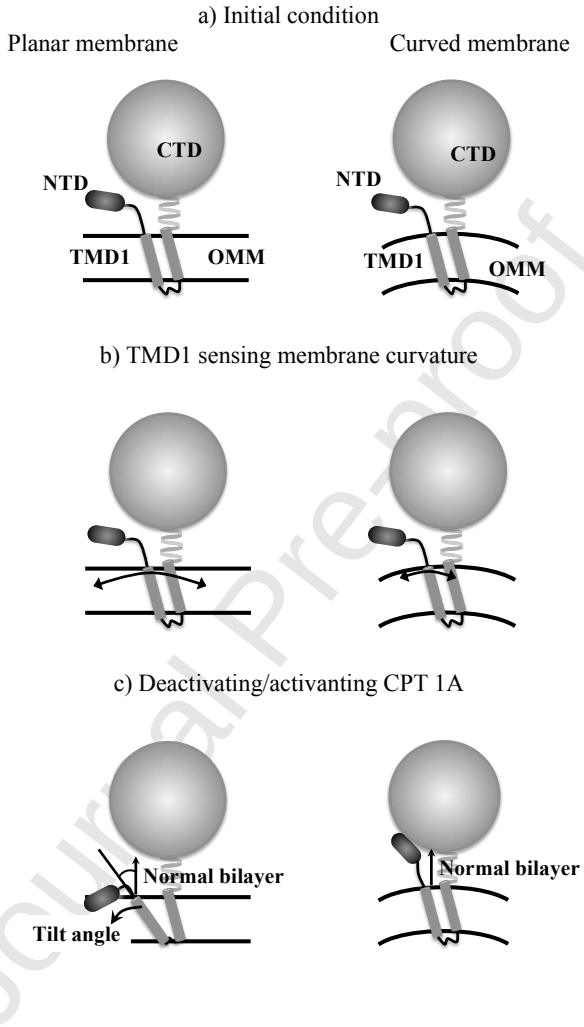

Figure 8: (a) Initial condition of the CPT 1A enzyme in presence of a planar (left) and curved (right) lipid bilayer. (b) The TMD1 begins to sense the curvature of the membrane by varying the tilt angle orientation, note that in the case of the planar membrane the tilt angle change much more than in the case of the curved membrane. (c) If the lipid bilayer is planar, the TMD1 moves toward the normal bilayer and the NTD is adsorbed deactivating the CPT 1A. If the lipid bilayer is curved, the TMD1 tilt angle orientation remains close to the normal bilayer and the NTD interacts with the CTD activating the enzyme.

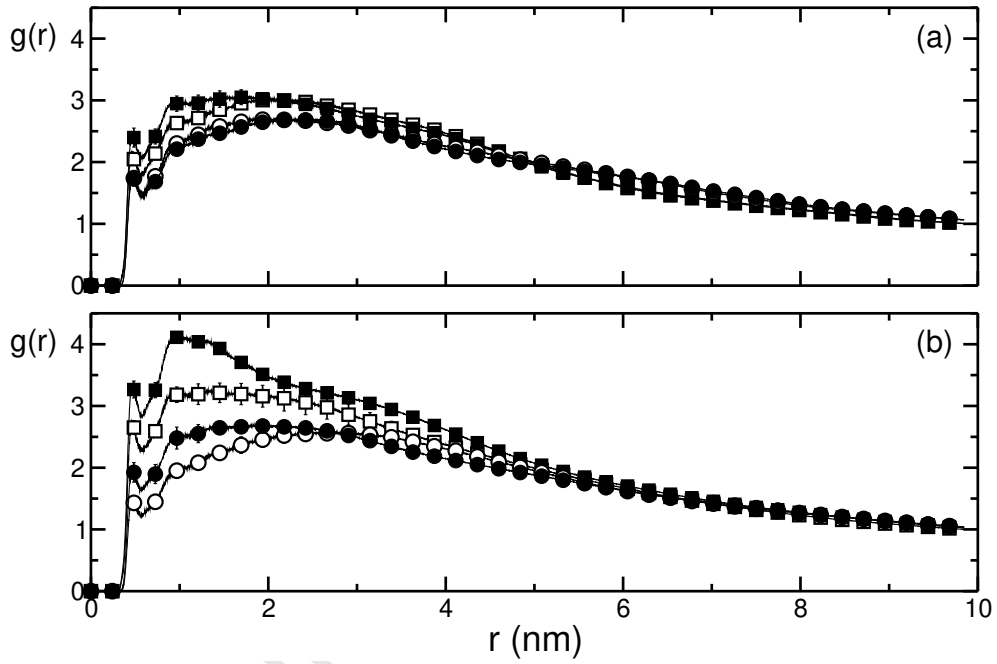

Figure 9: Radial distribution function of both types of lipids around the TMDs of the CPT 1A, for a: (a) a curved lipid bilayer and (b) a planar lipid bilayer. □ is for POPE for the first 150 ns, ■ is for POPE for the last 200 ns, ○ is for POPC the first 150 ns and ● is for POPC for the last 200 ns. Error bars represent the standard deviation calculations, which in some cases are the same size of the symbol.

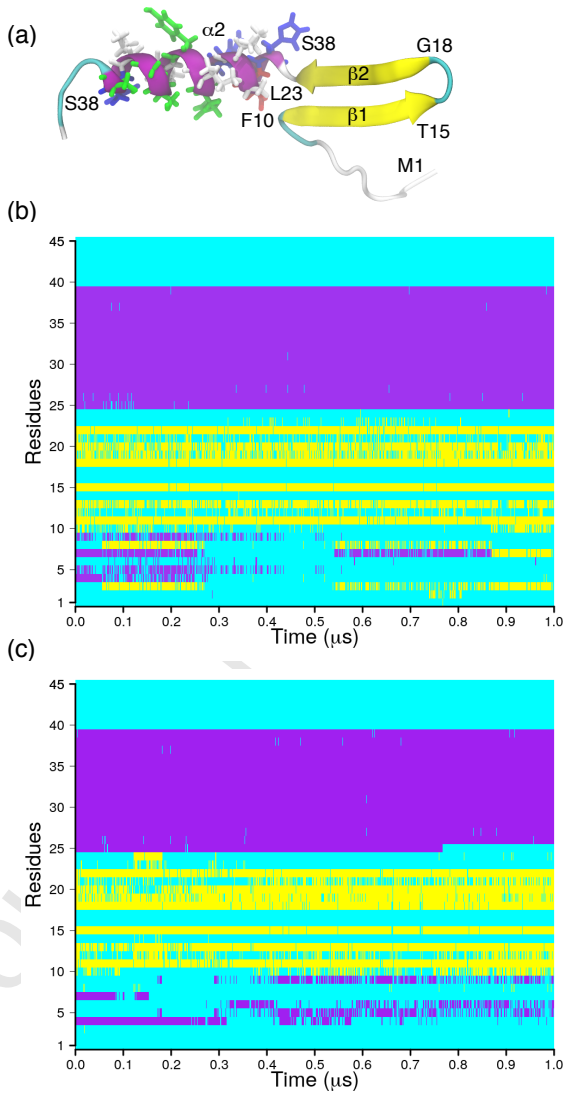

Figure 10: (a) Schematic representation of the NTD structure (PDB ID: 2LE3). The structures corresponding to $\beta 1$, $\beta 2$ and $\alpha 2$ are illustrated. Time evolution of the secondary structure of the residues belonging to the N-terminal of CPT 1A enzyme, in presence of a: (b) curved lipid bilayer and (c) planar lipid bilayer. Color: cyan coil, purple α-helix and yellow extended.

Graphical abstract

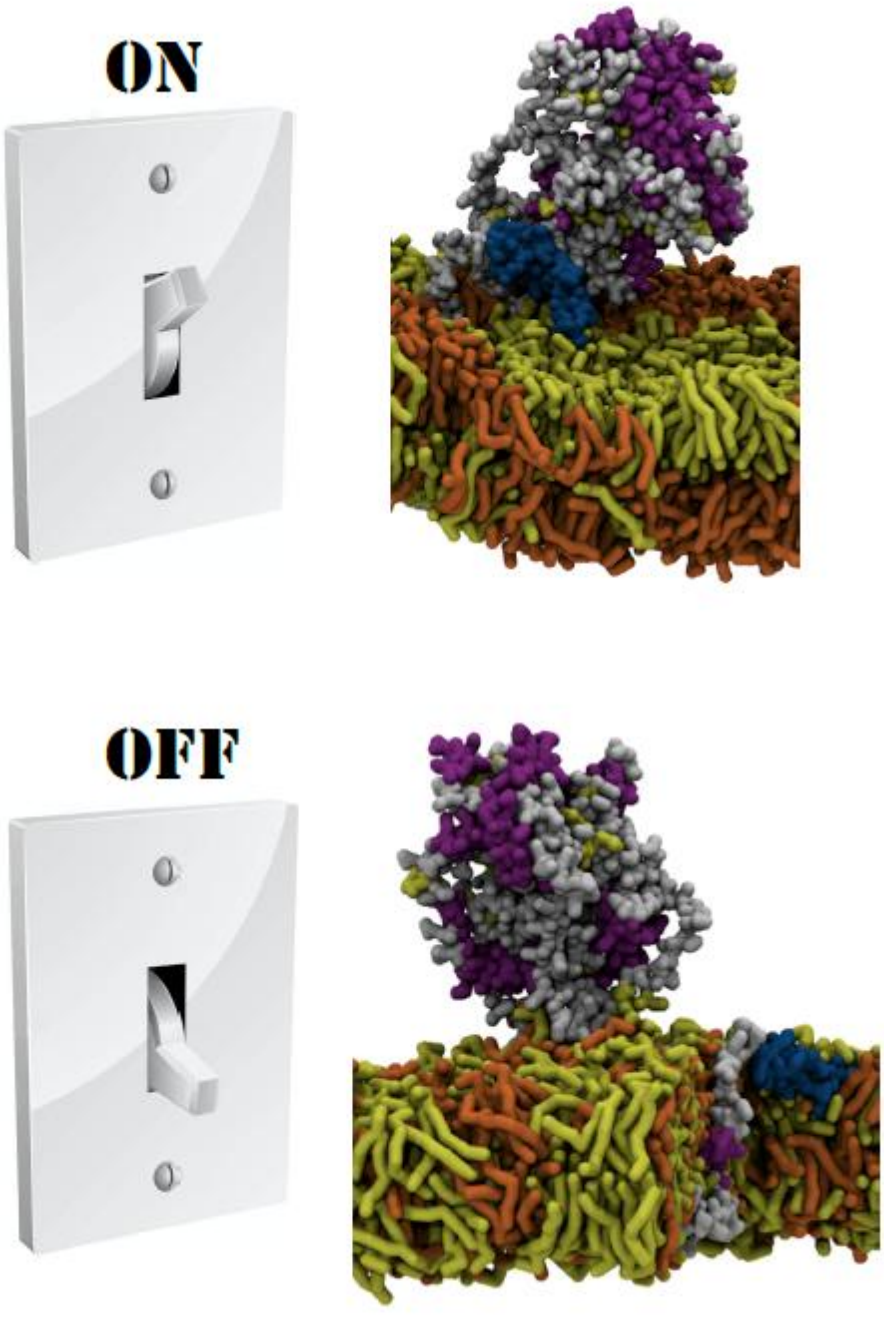

Highlights

- The activation/deactivation of CPT 1A depends on the membrane curvature
- Transmembrane Domain is the primary sensor of the membrane curvature
- N-Terminal interacts either with C-Terminal or outer mitochondrial membrane, depending on the structural membrane context